Marginalized particle filtering for reliable land vehicle navigation in global navigation satellite system-denied environments

Abdelkabir Lahrech[1], Aziz Soulhi[2]
[1]Multidisciplinary Laboratory of Research and Innovation (LMRI), Sultan Moulay Slimane University, Khouribga, Morocco
[2]Laboratory of Applied Mathematics and Decision Support Computing (LMAID), Superior National School of Mines, Rabat, Morocco

Article Info

Article history:

Received Aug 9, 2024
Revised Dec 18, 2024
Accepted Jan 16, 2025

Keywords:

Digital maps
GPS navigation
Marginalized filtering
Multisensor fusion
Non-linear filtering

ABSTRACT

Accurate localization in land vehicle navigation systems is highly dependent on the global navigation satellite system (GNSS). However, GNSS signal outages are common in urban areas due to obstacles such as tall buildings and tunnels. To mitigate these issues, digital road maps and dead reckoning sensors, like odometers, are often integrated to provide continuous vehicle localization. This paper presents a robust estimation method to solve the fusion problem of GNSS, odometer, and digital road map measurements in the presence of GNSS outages. The proposed solution utilizes a marginalized particle filter (MPF), which combines the robustness of particle filtering with the efficiency of a Kalman filter to handle the linear and non-linear parts of the state and/or measurement equations, respectively. When GNSS signals are unavailable, the MPF fuses all available pseudo-range data with odometric and map information to enhance vehicle positioning. The effectiveness of the proposed method is demonstrated using real-world data in an urban transportation scenario, highlighting significant performance improvements and real-time application potential.

Corresponding Author:

Abdelkabir Lahrech
Multidisciplinary Laboratory of Research and Innovation (LMRI), Polydisciplinary Faculty,
University of Sultan Moulay Slimane
Khouribga, Morocco
Email: a.lahrech@usms.ma

1. INTRODUCTION

In recent decades, the use of positioning and navigation technologies has significantly increased, especially in transportation applications. The global navigation satellite system (GNSS) is a fundamental component for many navigation systems due to its long-term stability and global coverage [1], [2]. However, in dense urban environments, GNSS performance can be compromised due to poor satellite visibility and signal blockages caused by tall buildings and tunnels. These challenges necessitate the use of supplementary sensors to ensure continuous and accurate vehicle positioning [3], [4]

Dead-reckoning (DR) sensors, such as odometers, are commonly used to provide continuous navigation support. Integrated into antilock braking systems (ABS), odometers generate digital pulses for each wheel revolution, allowing for distance estimation [5]. Additionally, digital road maps can enhance positioning accuracy through a process known as map-matching, which aligns the vehicle's estimated position with the road network. Many methods have been developed to solve the map-matching problem, employing topologic and geometric techniques such as point-to-point, point-to-arc, and curve-to-curve matching [6], [7]. However, these methods are susceptible to errors in dense road networks.

The extended Kalman filter (EKF) is frequently used to integrate GNSS data with measurements from odometers and low-cost inertial navigation systems (INS). However, the EKF's reliance on linearization can introduce significant estimation errors over time, and its assumption of Gaussian noise may not hold in non-linear, non-Gaussian contexts [8], [9]. In contrast, the unscented Kalman filter (UKF) uses a sampling technique to handle non-linearities and provides a more accurate approximation of the system's dynamic model, albeit at a higher computational cost [11], [10].

To address these limitations, recent advancements have focused on sequential Monte Carlo (SMC) methods, including the marginalized particle filter (MPF). These methods are capable of handling non-linear models and non-Gaussian statistics without requiring a linearization stage, as the EKF does. The MPF, in particular, is designed to reduce computational cost by applying particle filtering to the non-linear components of the state while using a Kalman filter for linear components [12]. This hybrid approach not only maintains high accuracy but also ensures computational efficiency, making it suitable for real-time applications [13]. Recent studies have shown the effectiveness of these methods in integrating GNSS with inertial navigation systems (INS) and other sensors to enhance vehicle localization accuracy in urban environments [14], [15].

This paper presents a marginalized particle filter (MPF) for land vehicle navigation in urban environments, where partial or total GNSS outages are common. During partial GNSS outages, the proposed method uses available pseudo-range data, even when fewer than four satellites are visible. In the event of total GNSS outages, the algorithm also incorporates dead-reckoning sensors and a digital road map to provide continuous localization. The MPF effectively solves the multi-sensor fusion problem by sequentially integrating measurements from all sensors to estimate the vehicle's 3D position. The proposed approach demonstrates significant improvements in both accuracy and computational efficiency, particularly in challenging urban environments.

2. VEHICLE SYSTEM AND SENSOR MEASUREMENT MODELING

2.1. Vehicle dynamics modeling

To address this estimation problem, we use a state model. The state vector $X_k = (x_k, y_k, z_k, v_k^x, v_k^y, v_k^z, \gamma_k^x, \gamma_k^y, \gamma_k^z)^T$ includes the 3-D components of the vehicle's position x, y, z, velocity v, and acceleration γ. The vehicle's dynamics are described using kinematic equations. Focusing on the x-component, we can write the equations as (1):

$$\begin{cases} \gamma_k^x &= \gamma_{k-1}^x + w_{\gamma_k^x} \\ v_k^x &= v_{k-1}^x + \gamma_{k-1}^x \Delta t + w_{v_k^x} \\ x_k &= x_{k-1} + v_{k-1}^x \Delta t + \frac{1}{2}\gamma_{k-1}^x \Delta t^2 + w_{x_k} \end{cases} \tag{1}$$

where $(w_{\gamma_k^x}, w_{v_k^x}, w_{x_k})$ are additive white Gaussian noise terms, and Δt represents the sampling interval. These equations can be expressed in matrix form as (2):

$$\begin{pmatrix} \gamma_k^x \\ v_k^x \\ x_k \end{pmatrix} = \begin{pmatrix} 1 & 0 & 0 \\ \Delta t & 1 & 0 \\ \frac{1}{2}\Delta t^2 & \Delta t & 1 \end{pmatrix} \begin{pmatrix} \gamma_{k-1}^x \\ v_{k-1}^x \\ x_{k-1} \end{pmatrix} + \begin{pmatrix} w_{\gamma_k^x} \\ w_{v_k^x} \\ w_{x_k} \end{pmatrix} \tag{2}$$

The same set of equations applies to the y and z components, allowing us to describe the overall vehicle dynamics with the following equation:

$$X_k = F X_{k-1} + W_k \tag{3}$$

where $W_k \sim N(0, Q_k)$ is a white Gaussian noise vector, and F is the dynamic transition matrix of the system, structured as:

$$F = \begin{pmatrix} F_x & \mathbb{0}_{3\times3} & 0_{3\times3} \\ \mathbb{0}_{3\times3} & F_y & \mathbb{0}_{3\times3} \\ \mathbb{0}_{3\times3} & \mathbb{0}_{3\times3} & F_z \end{pmatrix}$$

where each block F_x, F_y, and F_z corresponds to the dynamic transition sub-matrices for the x, y, and z components, respectively.

2.2. Measurement equations without satellite masking

When GPS data is available, the estimator incorporates these measurements to enhance the state estimation. The GPS measurement vector $\mathcal{Z}_k^{\text{GPS}} = (x_k^{\text{GPS}}, y_k^{\text{GPS}}, z_k^{\text{GPS}})^T$ is related to the state vector through the measurement function h^{GPS} and can be expressed as (4):

$$\mathcal{Z}_k^{\text{GPS}} = h^{\text{GPS}}(X_k) + V_k^{\text{GPS}} \tag{4}$$

where h^{GPS} is the measurement function and V_k^{GPS} is an additive white Gaussian noise with zero mean and covariance matrix R_k^{GPS}.

2.3. Measurement equations with partial GPS outages

When the number of available satellite signals is insufficient to compute a complete GPS position (i.e., fewer than 4 satellites), the filter utilizes the limited pseudorange measurements to compute the GPS position and estimate the vehicle's kinematic characteristics. For example, if only three satellites are visible, the GPS pseudorange equations Pr_k^j for the j-th satellite can be expressed as follows, neglecting various additional biases related to signal propagation (ionospheric and tropospheric delays):

$$Pr_k^j = \sqrt{(x_k - x_k^{s,j})^2 + (y_k - y_k^{s,j})^2 + (z_k - z_k^{s,j})^2} + c\delta_k \tag{5}$$

where (x_k, y_k, z_k) are the coordinates of the receiver's position, $(x_k^{s,j}, y_k^{s,j}, z_k^{s,j})$ are the coordinates of the j-th satellite, δ_k is the clock offset, and c is the speed of light.

The receiver's position and clock offset $(x_k, y_k, z_k, \delta_k)$ are unknown parameters that must be estimated. Typically, computing the receiver's location directly would require more than four pseudorange measurements. However, the proposed method leverages the available pseudorange measurements to estimate a partial GPS position $\mathcal{Z}_k^{\text{PGPS}}$ using the predicted state vector components and a non-linear least squares method to solve the system of equations.

Pseudorange measurements are initially computed in the earth-centered, earth-fixed (ECEF) coordinate system and then transformed into the Universal Transverse Mercator (UTM) coordinate system to be fused with odometric and map measurements. The partial GPS position can be described as (6):

$$\mathcal{Z}_k^{\text{PGPS}} = h^{\text{PGPS}}(X_k) + V_k^{\text{PGPS}} \tag{6}$$

where h^{PGPS} is the non-linear measurement function used in the pseudorange equations, and V_k^{PGPS} represents Gaussian white noise with zero mean and covariance R_k^{PGPS}.

2.4. Odometer measurement equations

When GPS data is unavailable, the differential odometry sensor is used to estimate the vehicle's position [16]. This sensor provides measurements $\mathcal{Z}_k^{\text{ODO}}$ of the elementary displacements of the left and right wheels [17]. The measurement vector is given by (7):

$$\mathcal{Z}_k^{\text{ODO}} = \begin{pmatrix} \Delta D_k^R \\ \Delta D_k^L \end{pmatrix} = h^{\text{ODO}}(X_k) + V_k^{\text{ODO}} \tag{7}$$

where (ΔD_k^R) and (ΔD_k^L) are the elementary displacements of the right and left wheels, respectively, and θ_k^{ODO} is the vehicle's orientation relative to the horizontal axis. The function h^{ODO} represents the odometry measurement function, and V_k^{ODO} is an additive white Gaussian noise with zero mean and covariance matrix R_k^{ODO}. The displacements for the right and left wheels can be expressed as (8):

$$\begin{cases} \Delta D_k^R = \dfrac{\sqrt{(\Delta D_k^{R,x})^2 + (\Delta D_k^{R,y})^2}}{r_R} + V_k^{\text{ODO,R}} \\ \Delta D_k^L = \dfrac{\sqrt{(\Delta D_k^{L,x})^2 + (\Delta D_k^{L,y})^2}}{r_L} + V_k^{\text{ODO,L}} \end{cases} \tag{8}$$

where r_L and r_R are the radii of the left and right wheels, respectively, and $(\Delta D_k^{L,x}, \Delta D_k^{L,y})$ and $(\Delta D_k^{R,x}, \Delta D_k^{R,y})$ are the vehicle's left and right displacements along the x and y components for each wheel. The relationship between these displacements and the components of the state vector can be expressed for both wheels as (9), (10):

$$\begin{cases} \Delta D_k^{R,x} = v_{k-1}^x \Delta k + \dfrac{e}{2}\left(\dfrac{v_k^y}{\| v_k \|} - \dfrac{v_{k-1}^y}{\| v_{k-1} \|}\right) \\ \Delta D_k^{R,y} = v_{k-1}^y \Delta k - \dfrac{e}{2}\left(\dfrac{v_k^x}{\| v_k \|} - \dfrac{v_{k-1}^x}{\| v_{k-1} \|}\right) \end{cases} \tag{9}$$

$$\begin{cases} \Delta D_k^{L,x} = v_{k-1}^x \Delta k - \dfrac{e}{2}\left(\dfrac{v_k^y}{\| v_k \|} - \dfrac{v_{k-1}^y}{\| v_{k-1} \|}\right) \\ \Delta D_k^{L,y} = v_{k-1}^y \Delta k + \dfrac{e}{2}\left(\dfrac{v_k^x}{\| v_k \|} - \dfrac{v_{k-1}^x}{\| v_{k-1} \|}\right) \end{cases} \tag{10}$$

where e is the distance between the left and right wheels. The odometry measurements provide an estimate of the vehicle's speed and direction, allowing for corrections to the vehicle's dynamics. However, it is important to note that these sensors can accumulate errors over time, leading to potential inaccuracies in the vehicle's estimated location.

2.5. Road map measurement equations

When GPS data is unavailable, the proposed filter also integrates measurements from a digital road map to enhance vehicle positioning. This road map is part of a geographic information system (GIS) and consists of roads represented by two-dimensional arcs composed of piecewise segments. Each segment is defined by a finite number of nodes, marking endpoints or transitions between segments. These nodes provide essential location coordinates $(x_k^{\text{MAP}}, y_k^{\text{MAP}})$ and orientation θ_k^{MAP}, which contribute to improving the vehicle's estimated location. The integration of the digital road map is modeled as a measurement equation, with the cartographic database serving as a set of potential candidates for this equation, thus enhancing positioning accuracy [18]. The road map measurement vector $\mathcal{Z}_k^{\text{MAP}} = (x_k^{\text{MAP}}, y_k^{\text{MAP}}, \theta_k^{\text{MAP}})$ includes the coordinates and direction of a segment and it is given by (11):

$$\mathcal{Z}_k^{\text{MAP}} = h^{\text{MAP}}(X_k) + V_k^{\text{MAP}} \tag{11}$$

where h^{MAP} is the map measurement function, V_k^{MAP} is an additive white Gaussian noise with zero mean and covariance matrix R_k^{MAP}. The equations for the map measurement function are:

$$\begin{cases} x_k^{\text{MAP}} &= x_k + V_k^{\text{MAP,x}} \\ y_k^{\text{MAP}} &= y_k + V_k^{\text{MAP,y}} \\ \theta_k^{\text{MAP}} &= \tan^{-1}\left(\dfrac{v_k^y}{v_k^x}\right) + V_k^{\text{MAP},\theta} \end{cases} \tag{12}$$

This modeling allows for the direct integration of road map errors and uncertainties via the map measurement noise statistics. Improved map measurements, combined with accurate cartographic data, significantly enhance vehicle localization, particularly in urban environments where GPS coverage is poor.

3. MARGINALIZED PARTICLE FILTERING

Marginalized particle filtering (MPF), also known as Rao-Blackwellization filtering is an advanced technique used to address the limitations of standard particle filters, especially in applications involving high-dimensional state spaces and nonlinear models. By marginalizing out the linear components of the state, MPF improves computational efficiency and estimation accuracy [19]. This section details the MPF approach and its application to vehicle navigation.

3.1. State model and marginalization

To address this estimation problem, we use a state model where the state vector is partitioned into components Λ_k (position and velocity) and Γ_k (acceleration). This partitioning allows us to treat the linear and non-linear components separately, improving the computational efficiency of the filtering process. The dynamics and measurement equations can be expressed as (13):

$$\begin{cases} \Lambda_k &= F^{\Lambda\Lambda}\Lambda_{k-1} + F^{\Lambda\Gamma}\Gamma_{k-1} + W_k^{\Lambda} \\ \Gamma_k &= F^{\Gamma\Gamma}\Gamma_{k-1} + W_k^{\Gamma} \\ \mathcal{Z}_k &= h(\Lambda_k) + V_k \end{cases} \tag{13}$$

where W_k^{Λ} and W_k^{Γ} are Gaussian white noises with zero mean and covariance matrices Q_k^{Λ} and Q_k^{Γ}, respectively. The measurement noise V_k is also a Gaussian white noise with zero mean and covariance matrix R_k. The matrices $F^{\Lambda\Lambda}$, $F^{\Lambda\Gamma}$, and $F^{\Gamma\Gamma}$ represent the relationships between the state components.

3.2. Proposed solution

Solving the dynamic state estimation requires determining the probability density function (PDF) of the state vector X_k, based on the observed measurements:

$$P(X_k|Z_k) = P(\Lambda_k, \Gamma_k|Z_k) \tag{14}$$

where S_k denotes the sequence $\{S_0, \ldots, S_k\}$, with S representing X, Z, Λ, Γ. Using Bayes' theorem, this PDF can be decomposed into two parts, corresponding to the linear and non-linear components of the state vector:

$$P(X_k|Z_k) = P(\Gamma_k|\Lambda_k, Z_k)P(\Lambda_k|Z_k) = P(\Gamma_k|\Lambda_k)P(\Lambda_k|Z_k) \tag{15}$$

The probability density function $P(\Lambda_k|Z_k)$, which addresses the non-linear component of the problem, is estimated using a particle filter. The recursive update is governed by Bayes' theorem:

$$P(\Lambda_k|Z_k) = \frac{P(Z_k|\Lambda_k)P(\Lambda_k|\Lambda_{k-1})}{P(Z_k|Z_{k-1})} P(\Lambda_{k-1}|Z_{k-1}) \tag{16}$$

The calculation of the conditional PDF $P(\Gamma_k|\Lambda_k)$ is performed under the assumption of known pose at each time instant. Let $Y_k = \Lambda_k - F^{\Gamma\Gamma}\Lambda_{k-1}$. The dynamics equations for the state model are linear and Gaussian:

$$\begin{cases} \Gamma_k &= F^{\Gamma\Gamma}\Gamma_{k-1} + W_k^{\Gamma}, \\ Y_k &= F^{\Lambda\Gamma}\Gamma_{k-1} + W_k^{\Lambda}. \end{cases} \tag{17}$$

Given the linear Gaussian nature of these equations, the optimal solution for acceleration estimation is provided by the Kalman filter.

The proposed algorithm for marginalized particle filtering involves the following steps:

a. Filter initialization parameters: The N particles X_0^i are initialized according to the priori distribution:

$$\Lambda_0^i \sim P(\Lambda_0), \qquad \Gamma_0^i \sim P(\Gamma_0), \qquad P_{0|0} = P_0 \tag{18}$$

b. Prediction: At each time step k, the Kalman filter estimates the 3-D acceleration parameters for each particle using all available measurements up to $k-1$.

$$\Gamma_{k|k-1}^i = F^{\Gamma\Gamma}\Gamma_{k-1|k-1}^i \tag{19}$$

$$P_{k|k-1} = F^{\Gamma\Gamma}P_{k-1|k-1}(F^{\Gamma\Gamma})^T + Q_k^{\Gamma} \tag{20}$$

c. Particles propagation: The particles are propagated through the state space based on the dynamics equation (13), generating N random sequences according to the distribution $P(W_k^{\Lambda})$.

$$\Lambda_k^i = F^{\Lambda\Lambda}\mathbf{\Lambda}_{k-1}^i + F^{\Lambda\Gamma}\Gamma_{k|k-1}^i + W_k^{\Lambda} \tag{21}$$

$$W_k^{\Lambda} \sim \mathcal{N}\left(0, F^{\Lambda\Gamma}P_{k|k-1}(F^{\Lambda\Gamma})^T + Q_k^{\Lambda}\right) \tag{22}$$

d. Updated estimation: The N Kalman filters are updated with the measurement using Λ_k^i and Λ_{k-1}^i:

$$Y_k^i = \Lambda_k^i - F^{\Gamma\Gamma}\Lambda_{k-1}^i \tag{23}$$

$$K_k = P_{k|k-1}(F^{\Lambda\Gamma})^T \left(F^{\Lambda\Gamma}P_{k|k-1}(F^{\Lambda\Gamma})^T + Q_k^{\Lambda}\right)^{-1} \tag{24}$$

$$\Gamma_{k|k}^i = \Gamma_{k|k-1}^i + K_k\left(Y_k^i - F^{\Lambda\Gamma}\Gamma_{k|k-1}^i\right) \tag{25}$$

$$P_{k|k} = P_{k|k-1} - K_k F^{\Lambda\Gamma} P_{k|k-1} \tag{26}$$

e. Weighting: The weighting step evaluates the probability associated with each particle using Bayes' rule. This step employs the available measurement $\mathcal{Z}_k$ at time k to compute the weight of each particle, p_k^i, according to (27):

$$p_k^i = \frac{\exp\left(-\frac{1}{2}\|\mathcal{Z}_k - h(\Lambda_k^i)\|_{R_k}^2\right)}{\sum_{j=1}^{N}\exp\left(-\frac{1}{2}\|\mathcal{Z}_k - h(\Lambda_k^j)\|_{R_k}^2\right)} p_{k-1}^i \tag{27}$$

where $\|\cdot\|_R^2 = (\cdot)^T R^{-1}(\cdot)$. R is the measurement noise covariance matrix.

This step calculates the weight of each particle by leveraging the available observation $\mathcal{Z}_k$ at time k. Depending on the GPS data availability, three main scenarios are considered:

– GPS measurements available: in this scenario, the filter utilizes GPS measurements exclusively to determine the vehicle's parameters, such as acceleration, velocity, and position. GPS data is considered available when pseudo-range measurements from at least four satellites are accessible. In such cases, the weights of the particles are determined based on the available GPS data to update the particle states accurately.

$$p_k^i = \frac{\exp\left(-\frac{1}{2}\|\mathcal{Z}_k^{\text{GPS}} - h^{\text{GPS}}(\Lambda_k^i)\|_{R^{\text{GPS}}}^2\right)}{\sum_{j=1}^{N}\exp\left(-\frac{1}{2}\|\mathcal{Z}_k^{\text{GPS}} - h^{\text{GPS}}(\Lambda_k^j)\|_{R^{\text{GPS}}}^2\right)} p_{k-1}^i \tag{28}$$

– Limited GPS availability: in the event of partial GPS outages, the available GPS pseudorange measures are used even if fewer than four satellites are in view, as they still contain positioning information. To avoid indetermination, the predicted localization parameters of the state vector are used to compute a GPS measurement using the filter. For instance, if only three GPS satellites are available, the pseudo-range equation can be expressed as (29):

$$Pr_k^j \quad = \quad \sqrt{(x_k^{s,j} - \hat{x}_{k|k-1})^2 + (y_k^{s,j} - y_k)^2 + (z_k^{s,j} - z_k)^2} + c\delta t \tag{29}$$

where $j = \{1,2,3\}$ and $\hat{x}_{k|k-1}$ represents the prediction of x_k calculated by the filter. To compute a partial GPS position $\mathcal{Z}_k^{\text{PGPS}}$, the predicted position $\hat{x}_{k|k-1}$ from the proposed filter, along with the least squares method, can be used when at least three pseudo-range measurements are available. When only two satellites are visible, the method requires using two components of the predicted state vector, $\hat{y}_{k|k-1}$ and $\hat{z}_{k|k-1}$, to solve the GPS navigation problem. This approach ensures that even with limited satellite visibility, the system can still provide accurate positioning by effectively leveraging the available data.

During periods of limited GPS availability, the filter also integrates odometer measurements along with data from digital road maps to estimate displacement. The primary challenge is aligning the previously predicted state with the map data. This involves matching the predicted location of the vehicle with the road network on the map.

There are several solutions to address the multitarget multisensor tracking problem. These solutions include probabilistic data association and multiple hypothesis tracking techniques [20], similitude function minimization, as well as approaches that utilize fuzzy logic and belief theory [21]. Moreover, Markov decision processes with reinforcement learning offer robustness against noisy data [22].

In our solution, we have opted for a probabilistic approach that employs the Mahalanobis distance as a coherence metric [23], [24]. This metric is calculated based on the 2-D predicted map position: $\hat{\mathcal{Z}}^{\text{MAP}}_{k|k} = h^{\text{MAP}}\left(\hat{X}^{i}_{k|k}\right)$ and each available map attribute, which includes the coordinates of nodes and the directions of segments: $\mathcal{Z}^{\text{MAP}}_{m}$, $m = \{1, ..., m_{max}\}$. These normalized distances $d_m = (\mathcal{Z}^{\text{MAP}}_{m}, \hat{\mathcal{Z}}^{\text{MAP}}_{k|k})$ are computed by using every node and considering the following two possible directions of the road:

$$d_{1,m} = \min_{m}\left[(\mathcal{Z}^{\text{MAP,1}}_{m} - \widehat{\mathcal{Z}}^{\text{MAP}}_{k/k})^{T}(\widetilde{P}^{\text{MAP}}_{k/k})^{-1}\left(\mathcal{Z}^{\text{MAP,1}}_{m} - \widehat{\mathcal{Z}}^{\text{MAP}}_{k/k}\right)\right] \tag{30}$$

$$d_{2,m} = \min_{m}\left[(\mathcal{Z}^{\text{MAP,2}}_{m} - \widehat{\mathcal{Z}}^{\text{MAP}}_{k/k})^{T}(\widetilde{P}^{\text{MAP}}_{k/k})^{-1}\ (\mathcal{Z}^{\text{MAP,2}}_{m} - \widehat{\mathcal{Z}}^{\text{MAP}}_{k/k})\right] \tag{31}$$

where $\mathcal{Z}^{\text{MAP,1}}_{m} = (x^{\text{MAP}}_{m}, y^{\text{MAP}}_{m}, \theta^{\text{MAP}}_{m})$ and $\mathcal{Z}^{\text{MAP,2}}_{m} = (x^{\text{MAP}}_{m}, y^{\text{MAP}}_{m}, \theta^{\text{MAP}}_{m} + \pi)$
$\widetilde{P}^{\text{MAP}}_{k/k}$ represents the error covariance of the two-dimensional predicted map measurement.
The most appropriate map data is identified by minimizing a distance criterion based on a predefined threshold, i.e.,

$$\mathcal{Z}^{\text{MAP}*}_{k} = \arg\min_{\mathcal{Z}^{\text{MAP}}}[d_{1m}, d_{2m}] \leq S$$

Assuming that each sensor's measurement noise is independent, the log-likelihood function of equation 27 can be reformulated as follows:

$$\|\mathcal{Z}^{\text{PGPS}}_{k} - h^{\text{PGPS}}(\Lambda^{i}_{k})\|^{2}_{R^{\text{PGPS}}} + \|\mathcal{Z}^{\text{ODO}}_{k} - h^{\text{ODO}}(\Lambda^{i}_{k})\|^{2}_{R^{\text{ODO}}} + \|\mathcal{Z}^{\text{MAP}*}_{k} - h^{\text{MAP}}(\Lambda^{i}_{k})\|^{2}_{R^{\text{MAP}}}$$

f. Estimation: The global estimated state is traditionally provided by aggregating the weighted contributions of all particles. This can be mathematically expressed as (32):

$$\hat{X}_{k|k} = \sum_{i=1}^{N} p^{i}_{k}\left[\left(\Lambda^{i}_{k}\right)^{T}, \left(\Gamma^{i}_{k|k}\right)^{T}\right]^{T} = \sum_{i=1}^{N} p^{i}_{k} X^{i}_{k} \tag{32}$$

g. Resampling and redistribution: To address the degeneracy problem in the marginalized particle filter, a resampling procedure is employed, duplicating particles with high weights and discarding those with low weights. We use multinomial resampling, where particles are selected based on their weights compared to a uniform distribution $[0, 1]$ [25]. The number of effective particles N_{eff} is kept below a threshold N_{thresh}, calculated as (33):

$$N_{\text{eff}} = \frac{1}{\sum_{i=1}^{N}\left(p^{i}_{k}\right)^{2}} < N_{\text{thresh}} \tag{33}$$

After resampling, the weights are normalized to $p^{i}_{k} = \frac{1}{N}$.

4. EXPERIMENTAL RESULTS

In this section, we present experimental results to quantify the advantages of the proposed marginalized particle filter (MPF) method. The experiments were conducted using a vehicle driven in an urban area in Calais, France. The test vehicle was equipped with a Novatel GPS receiver, which calculates the GPS positioning. The measurement campaign was conducted in an urban environment over a duration of 323 seconds. The vehicle reached a maximum speed of 16.5 meters/second (approximately 60 kilometers/hour). The speed varied significantly due to frequent accelerations and decelerations, as well as stop-and-go situations caused by traffic lights and pedestrians. There were two periods where GPS positioning was unavailable due to an insufficient number of visible satellites: the first period lasted 40 seconds and the second lasted 30 seconds. During these periods, the estimator used the available GPS pseudorange measurements, odometric measurements, and the road network database as shown in Figure 1.

The sensors used in the experiments have the following parameters: The GPS provides the vehicle's 3-D location at a frequency of 1 Hz when available, with an error covariance matrix set to $R^{\text{GPS}} =$

$[10\ \ 0\ \ 0; 0\ \ 10\ \ 0; 0\ \ 0\ \ 10]$. The tropospheric delay is corrected using the Goodman and Goad model and the ionospheric delay is adjusted with the Klobuchar model [26]. The odometer measurements are taken at a frequency of 1 Hz with an associated error covariance matrix given by $R^{\text{ODO}} = [0.5\ \ 0; 0\ \ 0.5]$. This matrix accounts for primary sources of error, such as wheel skids and variations in wheel pressure.

The road map is discretized into a 5 meter grid, with an error covariance matrix of $R^{\text{MAP}} = [25\ \ 0\ \ 0; 0\ \ 25\ \ 0; 0\ \ 0\ \ 0.1\ \text{(rad)}]$. This discretization accounts for quantization noise and facilitates matching within a wider neighborhood. The algorithm utilizes a total of $N = 1000$ particles with a resampling threshold set at $N_{\text{thresh}} = \dfrac{2N}{3}$.

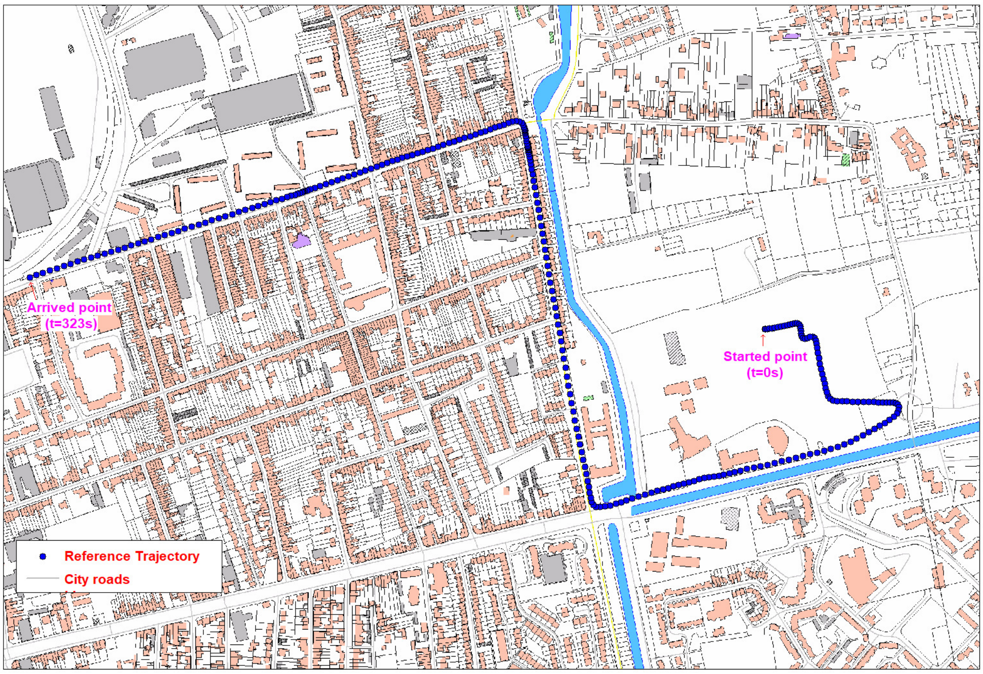

Figure 1. Reference trajectory of the vehicle

4.1. Vehicle trajectory estimation

This section, present the results of the proposed MPF applied to experimental data from a real urban transport scenario, focusing particularly on periods of GPS masking. During these periods, the filter utilizes the available pseudo-range data, odometric measurements, and the digital road map database to estimate the vehicle's trajectory. To evaluate the effectiveness of our MPF algorithm, we calculated the trajectory error using data collected from the differential GPS (DGPS) sensor.

Figures 2 and 3 show the velocity and acceleration errors in 3D for the vehicle, respectively. The GPS signal is partially unavailable, lasting 40 seconds, between $t = 104$ and $t = 144$. We observe that the joint use of the Dead Reckoning sensor and the digital road map database effectively bounds the velocity errors and accurately corrects the vehicle's dynamic characteristics, even when GPS data is unavailable. The MPF approach effectively constrains the kinematic errors when odometric data, partial GPS measurements, and digital road map data are used together.

4.2. Estimation of vehicle positioning

The marginalized particle filter shows enhanced accuracy in estimating the vehicle's 3-D positioning error, as illustrated in Figure 4. During the first period of partial GPS masking, which lasts 40 s from $t = 104$ s to $t = 144$ s, and the second period of partial GPS masking, lasting 30 s from $t = 249$ s to $t = 279$ s, the combination of partial GPS measurements, the DR sensor, and the digital road map data proves effective. This combination helps to bound the positioning errors and accurately corrects the vehicle's dynamic characteristics even in the absence of full or partial GPS data.

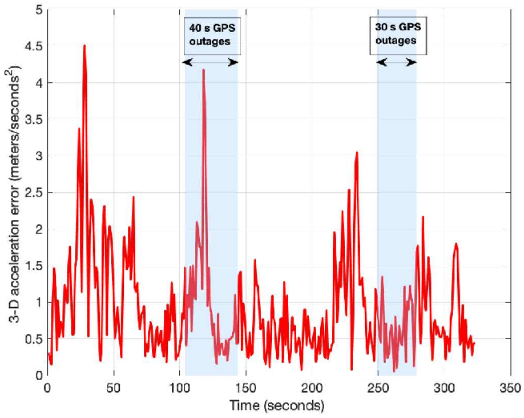

Figure 2. Vehicle's 3-D acceleration error across time

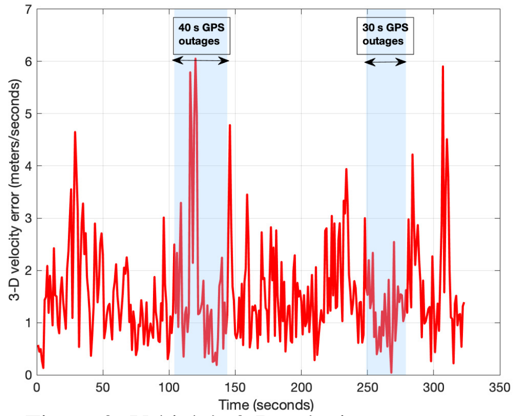

Figure 3. Vehicle's 3-D velocity error across time

Figure 5 illustrates the evolution of the global dilution of precision (GDOP), a key performance criterion for assessing GPS measurement quality, throughout the experiment. GDOP provides a measure of satellite geometry's impact on the accuracy of GPS positioning. During GPS outages, indicated by masking, neither GPS positions nor GDOP values can be calculated. The plot highlights periods of higher GDOP, notably from $t = 150$ to $t = 228$ and $t = 255$ to $t = 273$, which correspond to the degraded quality of the 3-D positioning estimations. This elevated GDOP indicates poor satellite geometry, resulting in less accurate GPS localization during these intervals. The figure also presents the visible satellite count during the sequence, providing additional context for interpreting the variations in GDOP.

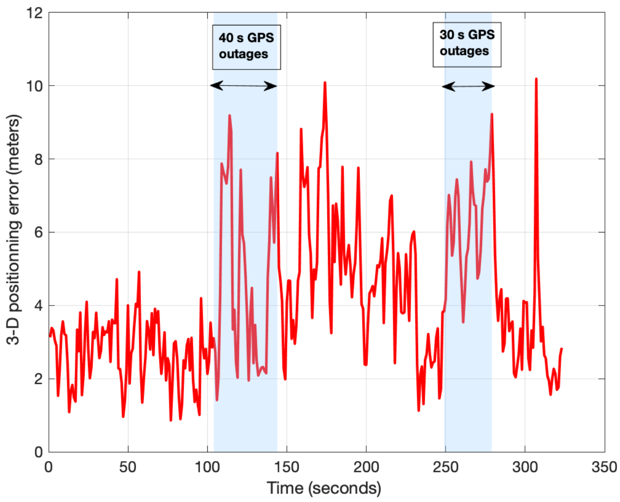

Figure 4. Vehicle's 3-D position error across time

During GPS outage periods, we also plotted the time evolution of the Mahalanobis distance, as shown in Figure 6. The values correspond to the minimum distances calculated from potential candidates. The map-matching threshold was experimentally set at $S = 7$.

Figure 7 displays the road network overlaid with various estimated trajectories of the land vehicle on a 2-D map. The estimated paths from different methods are plotted for comparison with the reference trajectory. The MPF estimated path is shown with red stars, representing the trajectory calculated using the MPF. The reference path is depicted in green, representing the vehicle's actual trajectory. The path estimated using dead reckoning (DR) methods is shown as an orange dotted line.

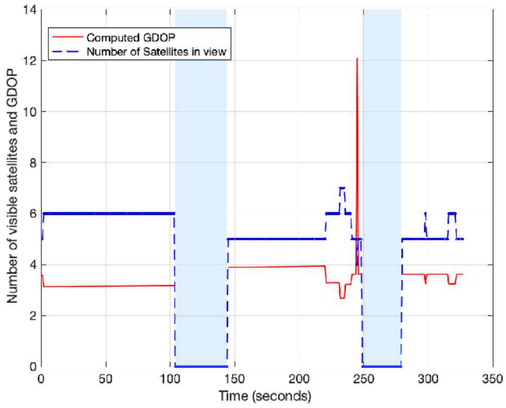

Figure 5. Evolution of GDOP and satellite visibility across time

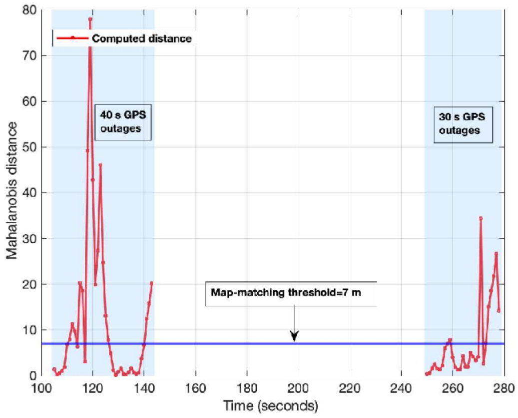

Figure 6. Map-matching criterion during the GPS outage

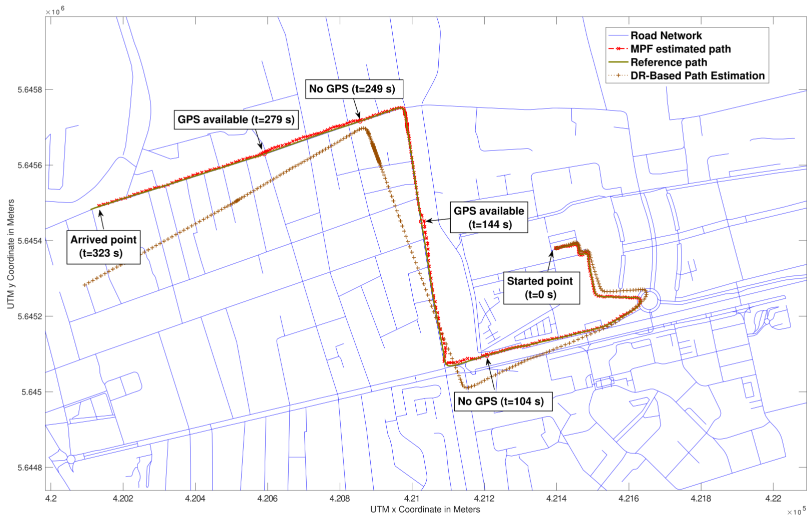

Figure 7. Comparison of true and estimated vehicle trajectories

The comparison reveals that both the MPF and DR-based paths closely follow the reference trajectory. However, the DR-based path diverges over time due to cumulative errors. In contrast, the MPF path aligns more accurately with the actual road network. This demonstrates the effectiveness of the map-tuned algorithm in reducing cumulative odometry errors, particularly during GPS outages. The improvement underscores the algorithm's ability to maintain precise vehicle localization by effectively integrating map data with GPS and DR measurements.

Table 1 provides a detailed summary of the mean errors and standard deviations for 3-D acceleration, velocity, and positioning during the GPS outages lasting $\Delta t_1 = 40$ seconds and $\Delta t_2 = 30$ seconds. The metrics are calculated for both individual outages and the entire period, reflecting the overall performance. The aggregated results clearly demonstrate that the proposed method consistently maintains superior positioning accuracy compared to DR-based navigation, particularly during GPS outages.

Table 1. Mean error and standard deviations during GPS masking periods ($\Delta t_1 = 40$ s and $\Delta t_2 = 30$ s)

Error type	Mean			Standard deviation		
	$\Delta t_1 = 40$ s	$\Delta t_2 = 30$ s	Total man	$\Delta t_1 = 40$ s	$\Delta t_2 = 30$ s	Total Std Dev
3-D Acceleration (m/s^2)	1.034810	0.674746	0.920335	0.875011	0.404364	0.712826
3-D Velocity (m/s)	1.702703	1.199478	1.559300	1.513326	0.594067	1.003898
3-D Positioning (m)	4.681527	6.212570	4.051459	2.352561	1.378975	1.970743

5. CONCLUSION

This paper presents a MPF approach to enhance vehicle localization in urban environments where GNSS outages are frequent. The approach integrates data from GNSS, odometric sensors, and digital road maps. The MPF efficiently addresses the sensor fusion problem, offering an optimal estimator due to the separation of state components in the filtering process.

In the absence of GNSS, the method effectively utilizes available pseudorange measurements, odometer data, and road map databases to accurately determine the vehicle's position. This approach allows for limiting positioning estimation errors that cannot be managed by odometer sensors alone. The benefits are demonstrated through a real-world urban scenario, confirming the reliability and effectiveness of the proposed method in maintaining accurate vehicle positioning when GNSS signals are unavailable. This approach can be utilized in a variety of transportation contexts, including traveler information systems, surveillance systems, and driver assistance, ensuring precise and continuous tracking of vehicle fleets.

FUNDING INFORMATION

The authors received no specific funding for this work.

AUTHOR CONTRIBUTIONS STATEMENT

This journal uses the Contributor Roles Taxonomy (CRediT) to recognize individual author contributions, reduce authorship disputes, and facilitate collaboration.

Name of Author	C	M	So	Va	Fo	I	R	D	O	E	Vi	Su	P	Fu
Abdelkabir Lahrech	✓	✓	✓	✓	✓	✓	✓	✓	✓	✓	✓			
Aziz Soulhi					✓					✓				

C	: **C**onceptualization	I	: **I**nvestigation	Vi	: **Vi**sualization
M	: **M**ethodology	R	: **R**esources	Su	: **Su**pervision
So	: **So**ftware	D	: **D**ata Curation	P	: **P**roject Administration
Va	: **Va**lidation	O	: Writing - **O**riginal Draft	Fu	: **Fu**nding Acquisition
Fo	: **Fo**rmal Analysis	E	: Writing - Review & **E**diting		

CONFLICT OF INTEREST STATEMENT

The authors declare no competing interests.

DATA AVAILABILITY

The data that support the findings of this study are available from the corresponding author, AL, upon reasonable request.

REFERENCES

[1] P. D. Groves, *Principles of GNSS, inertial, and multisensor integrated navigation systems*. Artech House, 2013.
[2] M. Tamazin, M. Karaim, and A. Noureldin, "GNSSs, signals, and receivers," in *Multifunctional Operation and Application of GPS*, R. B. Rustamov and A. M. Hashimov, Eds., IntechOpen, Rijeka, Croatia, 2018, ch. 6, pp. 69–85, doi: 10.5772/intechopen.74677.
[3] L. Gao, X. Xia, Z. Zheng, and J. Ma, "GNSS/IMU/LiDAR fusion for vehicle localization in urban driving environments within a consensus framework," *Mechanical Systems and Signal Processing*, vol. 205, p. 110862, 2023, doi: 10.1016/j.ymssp.2023.110862.
[4] H. Jiang, C. Shi, T. Li, Y. Dong, Y. Li, and G. Jing, "Low-cost GPS/INS integration with accurate measurement modeling using an extended state observer," *GPS Solutions*, vol. 25, no. 1, pp. 15, Jan. 2021, doi: 10.1007/s10291-020-01053-3.
[5] N. Dicu, G.-D. Andreescu, and E. Horatiu Gurban, "Automotive dead-reckoning navigation system based on vehicle speed and yaw rate," in *2018 IEEE 12th International Symposium on Applied Computational Intelligence and Informatics (SACI)*, Timisoara, Romania, 2018, pp. 225–228, doi: 10.1109/SACI.2018.8440954.
[6] J. Singh, S. Singh, S. Singh, and H. Singh, "Evaluating the performance of map matching algorithms for navigation systems: an empirical study," *Spatial Information Research*, vol. 27, pp. 63–74, 2019, doi: 10.1007/s41324-018-0214-y.
[7] L. Jiang, C. Chen, C. Chen, and B. Guo, "From driving trajectories to driving paths: a survey on map-matching algorithms," *CCF Transactions on Pervasive Computing and Interaction*, vol. 4, pp. 252–267, 2022, doi: 10.1007/s42486-022-00101-w.
[8] L. Zhao, W. Y. Ochieng, M. A. Quddus, and R. B. Noland, "An extended Kalman filter algorithm for integrating GPS and low cost dead reckoning system data for vehicle performance and emissions monitoring," *Journal of Navigation*, vol. 56, pp. 257-275, May 2003, doi: 10.1017/S0373463303002212.
[9] J. Liu and G. Guo, "Vehicle localization during GPS outages with extended Kalman filter and deep learning," *IEEE Transactions on Instrumentation and Measurement*, vol. 70, pp. 1-10, 2021, doi: 10.1109/TIM.2021.3097401.
[10] J. Cheng, D. Chen, R. Landry Jr., L. Zhao, and D. Guan, "An adaptive unscented Kalman filtering algorithm for MEMS/GPS integrated navigation systems," *Journal of Applied Mathematics*, vol. 2014, pp. 1-8, Mar. 2014, doi: 10.1155/2014/451939.
[11] M. R. Hidayatullah and J. -C. Juang, "Integrity on low-cost INS/GNSS/Odometer tightly coupled integration using extended and unscented Kalman filter," in *2022 International Automatic Control Conference (CACS)*, Kaohsiung, Taiwan, 2022, pp. 1-6, doi: 10.1109/CACS55319.2022.9969854.
[12] S. Jayamohan, S. N., and R. Kadarkaraiyandi, "A novel adaptive marginalized particle filter for mixed linear/nonlinear state-space models," *International Journal of Simulation: Systems, Science and Technology*, vol. 19, no. 6, pp. 54.1-54.15, Dec. 2018, doi: 10.5013/IJSSST.a.19.06.54.
[13] G. Hendeby, R. Karlsson, and F. Gustafsson, "The rao-blackwellized particle filter: a filter bank implementation," *EURASIP Journal on Advances in Signal Processing*, vol. 2010, 724087, 2010, doi: 10.1155/2010/724087.
[14] M. Shen, J. Sun, H. Peng, and D. Zhao, "Improving localization accuracy in connected vehicle networks using rao–blackwellized particle filters: theory, simulations, and experiments," *IEEE Transactions on Intelligent Transportation Systems*, vol. 20, no. 6, pp. 2255-2266, Jun. 2019, doi: 10.1109/TITS.2018.2866232.
[15] P.-J. Nordlund and F. Gustafsson, "Marginalized particle filter for accurate and reliable terrain-aided navigation," *IEEE Transactions on Aerospace and Electronic Systems*, vol. 45, no. 4, pp. 1385-1399, 2009, doi: 10.1109/TAES.2009.5310306.
[16] E. Abbott and D. Powell, "Land-vehicle navigation using GPS," *Proceedings of the IEEE*, vol. 87, no. 1, pp. 145–162, Jan. 1999, doi: 10.1109/5.736347
[17] C. Boucher, A. Lahrech, and J.-C. Noyer, "Non-linear filtering for land vehicle navigation with GPS outage," in *Proceedings of the 2004 IEEE International Conference on Systems, Man and Cybernetics (IEEE Cat. No.04CH37583)*, vol. 2, pp. 1321-1325, 2004, doi: 10.1109/ICSMC.2004.1399808.
[18] C. Boucher, A. Lahrech, and J.-C. Noyer, "Multisensor unscented filtering for GPS-based navigation systems," in *Proceedings of the 2007 IEEE Instrumentation and Measurement Technology Conference*, pp. 1–6, May 2007, doi: 10.1109/IMTC.2007.379130.
[19] R. Karlsson, T. Schon, and F. Gustafsson, "Complexity analysis of the marginalized particle filter," *IEEE Transactions on Signal Processing*, vol. 53, no. 11, pp. 4408-4411, 2005, doi: 10.1109/TSP.2005.857061.
[20] Y. Bar-Shalom and X. R. Li, "Multitarget multisensor tracking: principles and techniques," *Storrs, CT: YBS Publication*, 1995.
[21] M. E. El Najjar and P. Bonnifait, "A roadmap matching method for precise vehicle localization using belief theory and Kalman filtering," in *Proceedings of the 11th IEEE International Conference on Advanced Robotics*, July 2003, doi: 10.1007/s10514-005-0609-1.
[22] A. Wöltche, "Open source map matching with Markov decision processes: a new method and a detailed Benchmark with existing approaches," *Transactions in GIS*, vol. 27, pp. 1959–1991, Oct. 2023, doi: 10.1111/tgis.13107.
[23] K. Fukunaga and L. Hostetler, "Optimization of k-nearest neighbor density estimates," *IEEE Transactions on Information Theory*, vol. 19, no. 3, pp. 320–326, 1973, doi: 10.1109/TIT.1973.1055003.
[24] P. C. Mahalanobis, "On the generalised distance in statistics," *Sankhya A*, vol. 80, no. 1, pp. 1–7, 2018. Reprint of the original work from 1936, doi: 10.1007/s13171-019-00164-5.
[25] A. Doucet, N. de Freitas, and N. Gordon, "Sequential Monte Carlo methods in practice," *Journal of Computational and Graphical Statistics*, vol. 9, no. 3, pp. 251–262, 2000, doi: 10.1007/978-1-4757-3437-9_1
[26] J. A. Klobuchar, "Ionospheric time-delay algorithm for single frequency GPS user," *IEEE Transactions on Aerospace and Electronic Systems*, vol. 23, no. 3, pp. 325–331, 1987, doi: 10.1109/TAES.1987.310829.

BIOGRAPHIES OF AUTHORS

Abdelkabir Lahrech obtained his Ph.D. in signal processing, automatic, and computer science engineering in 2006 from the Université du Littoral Côte d'Opale (ULCO) in France. Since April 2009, he has been working as an assistant professor at the Faculté Polydisciplinaire de Khouribga, Sultan Moulay Slimane University, in Morocco. His research interests include non-linear and marginalized filtering, sequential Monte Carlo methods, and multisensor fusion, particularly as applied to intelligent transportation systems. He can be contacted at email: a.lahrech@usms.ma.

Aziz Soulhi is a professor at the National Superior School of Rabat in Morocco. He received his Ph.D. from the University of Lille in France. His research focuses on artificial intelligence applied to production and logistics systems. Currently, he serves as the president of the International Congress on Management and Systems Engineering and is the editor-in-chief of the International Journal of Management and Systems Engineering. He can be contacted at email: soulhi@enim.ac.ma.